International Journal of Pharmaceutics 646 (2023) 123476

Contents lists available at ScienceDirect

International Journal of Pharmaceutics

journal homepage: www.elsevier.com/locate/ijpharm

Excipient-free lyophilization of block copolymer micelles for potential lung surfactant therapy applications

Seyoung Kim [a,b,1], Sungwan Park [a,1], Daniel J. Fesenmeier [a], You-Yeon Won [a,c,*]

[a] Davidson School of Chemical Engineering, Purdue University, West Lafayette, IN 47907, United States
[b] Department of Polymer Science and Engineering, Dankook University, Yongin, Gyeonggi 16890, Republic of Korea
[c] Purdue University Institute for Cancer Research, Purdue University, West Lafayette, IN 47907, United States

ARTICLE INFO

Keywords:
Lyophilization
Acute respiratory distress syndrome
Polymer lung surfactant
Redispersibility
Polymer-brushed nanoparticles
Grafting density

ABSTRACT

Polymer lung surfactant (PLS) is a polyethylene glycol (PEG)-brushed block copolymer micelle designed for pulmonary surfactant replacement therapy. Saccharides (e.g., sucrose and (2-hydroxypropyl)-β-cyclodextrin) and water-soluble polymers (e.g., PEG), common excipients for lyophilization, were found to severely impair the surface activity of lyophilized PLS. To investigate the feasibility of excipient-free lyophilization of PLS, we studied the effects of both PLS material parameters and lyophilization operating parameters on the redispersibility and surface availability of reconstituted PLS, all without relying on excipients. We found that the redispersibility was improved by three factors; a faster cooling rate during the freezing stage reduced freezing stress; a higher PEG grafting density enhanced dissipating effects; and the absence of hydrophobic endgroups in the PEG block further prevented micelle aggregation. Consequently, the surface availability of PLS increased, enabling the micelle monolayer at the air/water interface to achieve a surface tension below 10 mN/m, which is a key pharmaceutical function of PLS. Moreover, the lyophilized micelles in powder form could be easily dispersed on water surfaces without the need for reconstitution, which opens up the possibility of inhalation delivery, a more patient-friendly administration method compared to instillation. The successful excipient-free lyophilization unlocks the potential of PLS for addressing acute respiratory distress syndrome (ARDS) and other pulmonary dysfunctions.

1. Introduction

Acute respiratory distress syndrome (ARDS) is a debilitating condition that impairs the function of lung surfactant, resulting in difficulty in breathing and severe reduction in blood oxygenation (Matthay and Zemans, 2011). In the United States, over 200,000 patients are diagnosed with ARDS annually, and it carries a high mortality rate of 25–40 % (Kim and Won, 2018; Sasannejad et al., 2019). Furthermore, ARDS has been identified as the leading cause of SARS-CoV-2-related deaths during the recent COVID-19 outbreak (Piva et al., 2021; Torres Acosta and Singer, 2020). ARDS is initiated by various types of lung injuries, such as inhalation of pathogens, pneumonia, and sepsis, and is exacerbated through a cascade of events that deactivate lung surfactant (Willson and Notter, 2011; Fan et al., 2018), which plays a crucial role in the breathing process (Dushianthan et al., 2012). In the early stages of ARDS, inflammation leads to pulmonary edema by increasing capillary permeability, causing surface-active plasma proteins like albumin and hemoglobin to enter the alveolar spaces (Matthay and Zemans, 2011; Dushianthan et al., 2012). Additionally, elevated levels of phospholipase A_2 (PLA_2) in ARDS lungs result in the accumulation of single-chain lysolipids and fatty acids by hydrolyzing double-chain phospholipids (Dushianthan et al., 2012; Barman et al., 2020). This deactivation mechanism undermines the efficacy of the current standard therapy, which involves replacing damaged lung surfactant with animal-extracted exogenous surfactant, as it is also susceptible to deactivation (Kim and Won, 2018; Willson and Notter, 2011; Willson et al., 2015). Consequently, there is an urgent need to discover and develop an artificial lung surfactant that is resistant to the deactivation mechanisms of ARDS.

Recently, we proposed a synthetic, non-phospholipid surface-active nanoparticle formulation that outperforms a commercial animal-extracted surfactant formulation (Infasurf®) in terms of reducing

* Corresponding author at: Davidson School of Chemical Engineering, Purdue University, West Lafayette, IN 47907, United States.
E-mail address: yywon@purdue.edu (Y.-Y. Won).
[1] Co-first authors.

https://doi.org/10.1016/j.ijpharm.2023.123476
Received 21 July 2023; Received in revised form 10 September 2023; Accepted 1 October 2023
Available online 5 October 2023

surface tension in the presence of bovine serum albumin (BSA) *in vitro* (Kim et al., 2018). This formulation, referred to as "polymer lung surfactant (PLS)," is based on micelles formed by amphiphilic block copolymers and exhibits enhanced resistance to the inhibitory effects of plasma proteins, as well as biological inertness in lung environments *in vivo* (Kim et al., 2022). Screening various block copolymers with chemically distinct hydrophobic blocks revealed that nanoparticles with highly hydrophobic vitrified cores, such as poly(styrene-*block*-ethylene glycol) (PS-PEG) and poly(*tert*-butyl methacrylate-*block*-ethylene glycol) (PtBMA-PEG), can mimic the surface mechanical behavior of the lung surfactant film by achieving near-zero surface tension (γ) and a sufficiently large compressibility modulus (E) (Kim et al., 2023). Subsequent comprehensive studies using mouse models of direct lung injuries demonstrated that PLS administration reduces inflammatory and hypoxia markers and improves lung compliance, thereby mitigating the amplification of lung permeability and acute inflammation during the pathological trajectory of ARDS (Fesenmeier et al., 2023).

Nevertheless, significant work remains to be done to transition from the proof-of-concept study to clinical trials of PLS, including formulation engineering and optimization of lung delivery. In particular, long-term storage of PLS at temperatures around 4 °C for more than 4 months, as well as prolonged exposure to ambient temperatures for over 5 days in normal saline solutions (0.9 % w/v), have been found to negatively affect the stability of the PLS formulation, leading to increased particle aggregation and a larger average particle size (Fesenmeier et al., 2023). These irreversible changes in the formulation result in decreased surface activity of PLS and a loss of its effectiveness in enhancing lung compliance (Fesenmeier et al., 2023). Therefore, it is critical to develop a suitable lyophilization and reconstitution procedure that allows for prolonged storage of PLS without any loss of efficacy.

Conventional lyophilization of nano-sized drug formulations often involves the use of excipients such as sugars and short-chain hydrophilic polymers as cryoprotectants or lyoprotectants protecting the active ingredients from the mechanical stresses caused by ice crystallization and drying forces (Abdelwahed et al., 2006; Miller et al., 2013; Sim et al., 2018). However, it is necessary to address the potential adverse effects of remaining excipients in a readily reconstituted PLS formulation on surface activity, such as competitive adsorption to the water surface (Arboleya and Wilde, 2005) or promoting solvation of the adsorbed micelles (Saenger and Müller-Fahrnow, 1988; Antipova et al., 1999). Alternatively, excipient-free lyophilization can be an ideal choice for preserving the surface activity of PLS. Previously, the lyophilization process without the use of excipients has been demonstrated with branched polymer-based nanoparticles (Logie et al., 2014; Zhao et al., 2017). However, it is unclear whether this approach can be applied to linear block copolymers.

This study focuses on the material and process design to successfully preserve the surface activity of model PLS formulations throughout the lyophilization and reconstitution processes. Three candidate materials with different "core-forming" hydrophobic block and end group chemistries (PS-PEG-OH, PS-PEG-OCH_3, and PtBMA-PEG-OCH_3) were used. Each block was designed to have a consistent molecular weight of ~ 5 kDa to eliminate any interference from molecular weight effects between different polymers. The first part of the study examines the detrimental effects of common excipients on the surface mechanical properties of PS-PEG-OH micelles. The second part explores process parameters for optimized excipient-free lyophilization of PS-PEG-OH micelles. The third part investigates the effects of PEG grafting density and polymer chemistries (i.e., the core block and end group) on the redispersibility and surface activity of lyophilized micelles. Lastly, the fourth part discusses the role of PEG brushes in reducing the mechanical stress and preventing the micelle aggregation by freeze-and-thaw calorimetric measurements. We demonstrate that a careful selection of materials and process parameters enables excipient-free lyophilization and subsequent long-term storage of PLS formulations without compromising colloidal stability and therapeutic activity, which lays the foundation for conducting IND-enabling studies on this innovative pharmaceutical.

2. Materials and methods

2.1. Materials

PS-PEG-OH, synthesized via anionic polymerization, was purchased from Polymer Source (Quebec, Canada). The number-average molecular weight (M_n) of each block and the overall molecular weight polydispersity index (M_w/M_n) are available in Table 1. Anhydrous styrene (Sigma Aldrich) and *tert*-butyl methacrylate (Sigma Aldrich) monomers were purified using activated alumina columns (Sigma Aldrich) to remove free radical inhibitors prior to the polymerization reactions. Sucrose (Sigma Aldrich), poly(ethylene glycol) monomethyl ether (PEG-OCH_3, M_n = 2,000 and 5,000 g/mol, Sigma Aldrich), and (2-hydroxypropyl)-β-cyclodextrin (HPβCD, Sigma Aldrich) were used as lyophilization excipients in their as-received form.

2.2. Polymer synthesis and characterization

For the Reversible Addition–Fragmentation Chain Transfer (RAFT) polymerization of amphiphilic block copolymers, PEG-OCH_3 of M_n = 5,000 g/mol was first conjugated with 4-cyano-4-[(dodecylsulfanylthiocarbonyl)sulfanyl]pentanoic acid (CDSP) by Steglich esterification in the presence of 4-dimethylaminopyridine and *N,N'*-dicyclohexylcarbodiimide in dichloromethane following our previous procedure (Kim et al., 2018). The synthesized macro-RAFT agent (CDSP-PEG-OCH_3) was isolated by triple precipitations in cold hexane and dried under vacuum overnight for 24 h. The dried CDSP-PEG-OCH_3 was co-dissolved with 2,2′-azobis(isobutyronitrile) in anhydrous 1,4-dioxane, and the solution was degassed via three freeze–pump–thaw cycles. Then, purified monomers were transferred into the mixture to initiate the RAFT polymerization. The polymerization reaction was run for 20 h at 75 °C and terminated by exposing the reaction mixture to air. The products, PS-PEG-OCH_3 and PtBMA-PEG-OCH_3, were triply precipitated in a 1:1 volumetric mixture of hexane and diethyl ether and dried under vacuum.

The number-average degrees of polymerization (DP_n) were characterized by ^{1}H NMR in CD_2Cl_2 solvent for PS-PEG-OCH_3 and $CDCl_3$ solvent for PtBMA-PEG-OCH_3. The DP_n of the hydrophobic PS and PtBMA blocks were calculated from the ratio of ^{1}H NMR peak areas between the ether protons of PEG (4.2–3.3 ppm) and specific protons of PS or PtBMA (Figures S1–S2 of Supplementary Material). The overall molecular polydispersity indices (M_w/M_n) of the block polymers were measured by gel permeation chromatography (GPC) which was calibrated with PS standards (Figure S3). The molecular characteristics of all block copolymers studied are summarized in Table 1.

2.3. PLS formulation and characterization

Block copolymer micelles with differing chemistry and sizes were prepared via a two-step solvent exchange technique termed as the Equilibration-Nanoprecipitation (ENP) method (Fesenmeier et al., 2022). 50 mg of each polymer was dissolved in a 5-mL mixture of

Table 1
Molecular characteristics of block copolymers. [a)] Overall molecular weight polydispersity index (M_w/M_n) obtained from gel permeation chromatography (GPC).

Sample name	PEG block end group	$M_{n,core}$ (g/mol)	$M_{n,PEG}$ (g/mol)	M_w/M_n[a)]
PS-PEG-OH	–OH	5,200	5,500	1.11
PS-PEG-OCH_3	–OCH_3	5,150	5,000	1.23
PtBMA-PEG-OCH_3	–OCH_3	6,080	5,000	1.19

acetone and Milli-Q water at varying solvent compositions (namely, the volume fraction of water, $\varphi_{w,ENP}$), and each solution was sonicated for complete homogenization and subsequently equilibrated at ambient temperature for 24 h. During the equilibration process, block copolymers self-assemble into spherical micelles near to equilibrium, and their size typically increases with $\varphi_{w,ENP}$ due to a greater solvent quality selectivity (Fesenmeier et al., 2022). To completely remove the acetone from the solution after the equilibration, the solution was transferred to a dialysis bag (Spectra/Por 7, 50 kDa molecular weight cutoff) in 1 L of water reservoir, and the dialysate was changed three times with fresh water over 48 h. The final concentration of the aqueous micelle dispersion was adjusted to 5 mg/mL by adding fresh Milli-Q water.

Micelles formulated using the ENP method were characterized by transmission electron microscopy (TEM) using a 200-kV Tecnai T20 instrument. Diluted suspensions in Milli-Q water (0.1 mg/mL) were negatively stained by mixing them in a 1:1 ratio (v/v) with a 1 % aqueous uranyl acetate solution and then dried on a carbon-coated grid that had been pre-treated by glow discharge. The average diameter of micelles measured from the TEM images were regarded as the apparent core diameter (D_c), from which the dimensionless PEG grafting density ($\sigma_{PEG} = pR_{g,PEG}^2/D_c^2$), defined as the ratio of the cross-section area of a PEG chain ($\pi R_{g,PEG}^2$) to the interfacial area per chain in the micelle ($\pi D_c^2/p$), was calculated. $R_{g,PEG}$ is the radius of gyration of an unperturbed PEG chain with an equivalent molecular weight in water (Kawaguchi et al., 1997). $p = (\pi D_c^3/6)(M_{n,core}/N_A\rho_{core})^{-1}$ is the aggregation number (where $M_{n,core}$ is the number-averaged molecular weight of the hydrophobic core block), N_A the Avogadro number, and ρ_{core} the density of the core block.

The average hydrodynamic diameter (D_h) distribution, the *z*-average hydrodynamic size ($<D_h>$), and the polydispersity index (*PDI*) of the micelle sizes before ("pristine") and after the lyophilization and reconstitution processes ("reconstituted") were measured by dynamic light scattering (DLS) using a Brookhaven NanoBrook 90Plus instrument. The nanoparticle solution was diluted to 0.5 mg/mL in Milli-Q water and filtered through a poly(tetrafluoroethylene) (PTFE) syringe filter 0.45 μm pores. The DLS measurements were performed at a scattering angle of 90° and a laser wavelength of 640 nm. The characteristics of the micelles studied are summarized in Table 2.

2.4. Lyophilization and reconstitution

2 mL of each micelle formulation was transferred into a 10-mL lyophilization vial equipped with a rubber stopper. Typically, a total of 18 vials (3 polymers × 2 ENP conditions × 3 replicates) or more were placed inside the chamber of a small-batch lyophilizer (MicroFD, Millrock Tech) with programmable thermal profiles. The lyophilization process followed a typical sequence; the solutions were rapidly cooled from 25 °C to the target shelf temperature (T_{shelf}) and then allowed to equilibrate for 3 h (the freezing stage). Subsequently, the frozen water (ice) was sublimated at a T_{shelf} below the eutectic temperature of the PEG/water system (–19 °C) until the chamber vapor pressure (*P*) reached the target pressure of 70 mTorr (the primary drying stage). Finally, the bound water was dried at a T_{shelf} above the triple point of water (0.01 °C) until the target pressure of $P = 70$ mTorr was achieved again (the secondary drying stage). Two different operating methods with distinct ramping rates and target T_{shelf} values were utilized, and the specific operational parameters used can be found in Table 3. Throughout the lyophilization process, real-time monitoring was conducted for T_{shelf}, *P*, and the heat flux between the vials and the shelf. For reconstitution, 2 mL of Milli-Q water was added to each vial containing lyophilized samples, followed by gentle shaking for 3 min and sonication for 3 min (Di Tommaso et al., 2010).

2.5. Surface mechanical analysis

The surface pressure–area (*Π–A*) isotherms of the micelle monolayers were measured using a Langmuir trough (KSV 5000, Biolin scientific) with two symmetric barriers attached at each end. The trough and two barriers were initially cleaned with ethanol and water three times. A total of 1.4 L of Milli-Q-purified water was poured in the trough, and a piece of filter paper was used as a Wilhelmy plate to measure the surface tension. Before each measurement, the water surface was aspirated to remove any interfacial contaminants ensuring that the surface pressure of pure water at maximum compression ($A = 71$ cm^2) did not exceed 0.2 mN/m.

Onto the clean surface of water at the maximum area (782 cm^2), 100 μL of the "pristine" or "reconstituted" micelle solution (5 mg/mL) was spread using a microsyringe. Droplets of a few microliter was formed on a tip of the syringe needle and carefully contacted on the water surface to spread the sample on the water. For the *Π–A* isotherm measurements of the PLS with added excipients, the excipients were added into the pristine solutions to achieve a 10 % w/v excipient concentration before the spreading. For the *Π–A* isotherms of the solid lyophilizates, 1.5 mg of the foamy solid was carefully placed piecewise on the clean water surface using a dressing forcep.

2.6. Differential scanning calorimetry (DSC)

Freezing and melting of the micelle formulations were analyzed using differential scanning calorimetry (DSC; DSC 4000, Perkin Elmer). A micelle concentration of ~ 100 mg/mL (i.e., ~20 times higher than the concentration of standard formulations) was used to precisely evaluate the amount of bound water to the PEG brushes. To increase the concentration, 0.5 mL of the pristine micelle formulation (at 5 mg/mL) was transferred into in a pre-rinsed centrifugal dialysis membrane tube (Amicon Ultra–0.5, MWCO 10 kDa) and centrifuged at 14,000 rpm for

Table 2
Structural characteristics of micelles. (a) Volume fraction of water used in the equilibrium nanoprecipitation (ENP) method. (b) Non-dimensionalized PEG grafting density. (c) Size increasing factor, i.e., hydrodynamic diameter ratio of reconstituted micelles to pristine micelles. (d) Surface availability.

Polymer	$\varphi_{w,ENP}$ [a]	Pristine				Reconstituted after Lyophilization			
		D_c (nm)	σ_{PEG} [b]	D_h (nm)	*PDI*	D_h (nm)	*PDI*	*SIF* [c]	*SA* [d]
PS-PEG-OH	0.2	13.3	7.1	47.1	0.300	131.6	0.158	2.79	0.36
	0.3	17.0	9.0	29.4	0.220	131.7	0.148	4.48	0.23
	0.5	19.3	10.2	31.2	0.082	59.2	0.151	1.90	0.87
	0.6	21.3	11.3	35.6	0.112	69.7	0.166	1.96	0.81
PS-PEG-OCH_3	0.1	14.8	8.0	26.8	0.177	152.1	0.141	5.68	0.09
	0.2	18.4	9.9	26.3	0.098	160.6	0.091	6.11	0.30
	0.3	18.9	10.2	28.8	0.029	158.9	0.170	5.52	0.25
	0.5	19.5	10.5	168.1	0.190	193.5	0.121	1.15	~4
PtBMA-PEG-OCH_3	0.1	16.5	7.8	32.0	0.218	155.5	0.189	4.86	0.14
	0.2	17.4	8.3	26.1	0.114	152.9	0.188	5.86	0.13
	0.3	19.9	9.4	27.5	0.082	109.6	0.133	3.99	0.18
	0.5	23.3	11.1	91.2	0.284	168.2	0.212	1.84	0.45

Table 3
Operating parameters for the lyophilization of PS-PEG-OH micelles formulated at $\varphi_{w,ENP} = 0.6$ and the reconstitution results. [a] Cooling or heating rate. [b] Shelf temperature. [c] Size increasing factor.

Method	Formulation Volume (mL)	Freezing Stage		Primary Drying Stage		Secondary Drying Stage		Reconstituted after Lyophilization		
		R (°C/min) [a]	T_{shelf} (°C) [b]	*R* (°C/min) [a]	T_{shelf} (°C) [b]	*R* (°C/min) [a]	T_{shelf} (°C) [b]	$\langle D_h \rangle$ (nm)	*PDI*	*SIF* [c]
A	38	–2	–60	+2	–30	+1	25	69.5	0.18	1.95
B	12	–1	–50	+1	–35	+1	25	82.3	0.17	2.40

20 min. The micelle concentration post centrifugation was measured using GPC by taking an aliquot of the concentrated micelle suspension. The GPC intensity peak area was converted to concentration using a calibrated data drived from a standard solution with a known polymer concentration. The precise concentrations of the micelle suspensions used in DSC are detailed in Table 4.

8 μL of the concentrated solution was transferred to a hermetically sealed DSC pan. A DSC cycle involving cooling from 30 °C to –50 °C and then reversing the heating back to 30 °C was carried out at with a ramp rate of 5 °C/min. The mass of eutectic PEG ($m_{PEG,eu}$) was calculated from the measured endothermic peak area (Q_{eu}) at the eutectic point according to

$$Q_{eu} = m_{eu}\Delta H_{eu} = (m_{PEG,eu}/w_{PEG,eu})\Delta H_{eu} \quad (1)$$

where $\Delta H_{eu} = 142 \pm 1$ J/(g eutectic mixture), determined through linear fits of the enthalpies of fusion of the PEG/water eutectic mixtures (Fig. 7 (b) and (c) from Ref. (Huang and Nishinari, 2001) and $w_{PEG,eu}$ (= 0.47) represents the mass fraction of PEG at the eutectic point (T_{eu} = –19 °C) (Kuttich et al., 2020). As a portion of PEG segments undergo dehydration to cover the surface of the hydrophobic core (Kim et al., 2018), it is important to note that only the remaining (hydrated) PEG segments have the capacity to form a eutectic mixture with the surrounding water. The fraction of hydrated PEG, $f_{hyd} = m_{PEG,eu}/m_{PEG}$, was evaluated from Eq. (2),

$$\Delta H_{eu:PEG} = Q_{eu}/m_{PEG} = [m_{PEG,eu}/(w_{PEG,eu}m_{PEG})]\Delta H_{eu} = (f_{hyd}/w_{PEG,eu})\Delta H_{eu} \quad (2)$$

where m_{PEG} is the total mass of PEG in the sample, and $\Delta H_{eu:PEG}$ is the enthalpy of fusion at the eutectic point per total mass of PEG. $\Delta H_{eu:PEG}$ and f_{hyd} values for each sample are provided in Table 4.

3. Results and discussion

3.1. Surface mechanics of PS-PEG-OH micelles in the presence of excipients

Excipients are commonly added to prevent structural damage and irreversible aggregation of nanoparticulate drugs caused by freezing and drying stresses, which result from ice crystallization and solvent sublimation, respectively, in conventional lyophilization processes (Trenkenschuh and Friess, 2021). These excipients are typically amphiphilic molecules that can interact favorably with both water (through hydrogen bonding) and particle surfaces (through van der Waals interactions) (Fonte et al., 2016). However, due to this amphiphilic nature of excipients, they can have detrimental effects on the surface activity of block copolymer micelle formulations, either by modifying the surface energy of hydrophobic micellar cores or by competitively adsorbing at the air–water interface. To examine the effect of excipients on the surface mechanical behavior of the model PLS formulation prior to the lyophilization study, we selected two saccharides (sucrose and HPβCD) and two hydrophilic polymers (2 and 5 kg/mol PEG-OCH_3) as representative excipients. A concentration of 10 % w/v, which falls within the typical range of 5–20 % w/v for optimal protection, (Saez et al., 2000; Lee et al., 2009; Suksiriworapong et al., 2014) was used.

Fig. 1 compares the surface pressure–area (Π–A) isotherms of PS-PEG-OH micelles formulated at $\varphi_{w,ENP} = 0.6$ with and without excipients. Here, the surface pressure ($\Pi = \gamma_0 - \gamma$), defined as the decrement in surface tension from that of pure water (γ_0 = 72 mN/m), is plotted against the trough area (A). The chosen model formulation exhibited the ability to achieve low surface tension ($\gamma < 10$ mN/m) upon compression of the surface, as demonstrated by the control isotherm. Strikingly, the addition of any excipient to the PS-PEG-OH formulation resulted in the loss of surface activity, preventing the attainment of high Π values. It is speculated that saccharides and PEG-OCH_3 excipients reduce the surface activity of PS-PEG-OH micelles in different ways. Consistent with our previous study, the isotherms of the saccharide-containing formulations resemble the typical surface mechanical behavior of block copolymer micelles with weakly hydrophobic cores, such as poly(*D,L*-lactic acid-*block*-ethylene glycol) (PLA-PEG) (Kim et al., 2023). This suggests a possible reduction in the interfacial tension between water and the hydrophobic PS core due to the mediating effect of influence, in line with existing literature on the favorable interactions between sucrose and globular proteins (Antipova et al., 1999; Chang et al., 2005).

On the other hand, PEG-OCH_3 excipients compete with the adsorption of PS-PEG-OH micelles at water surfaces. The maximum Π values of

Table 4
DSC characterization of concentrated aqueous micelle suspensions. [a] Volume fraction of water used in the Equilibration-Nanoprecipitation (ENP) method. [b] Weight fraction of polymer in the concentrated suspension (prepared via centrifugation) determined via GPC. [c] Freezing point. [d] Eutectic peak melting point and the enthalpy of fusion per gram of PEG in the system. [e] Hydrated PEG fraction, defined as the ratio of the PEG segments contained in the eutectic mixture to the total PEG in the system. [f] Melting point of the bulk water. [g] Aggregation of micelles leading to loss of micelles in the concentrated suspension (prepared via centrifugation).

Polymer	$\varphi^{a)}_{w,ENP}$	$w_{p,analyte}$ [b]	T_f (°C) [c]	T_{eu} (°C) [d]	$\Delta H_{eu:PEG}$ (J/g PEG) [d]	f_{hyd} [e]	T_m (°C) [f]
PS-PEG-OH	0.2	0.10	–15.6	–15.6	38	0.12	8.7
	0.3	0.08	–15.1	–16.5	28	0.09	8.4
	0.5	0.09	–13.7	–16.3	50	0.16	8.1
	0.6	0.06	–12.6	–15.9	84	0.27	8.9
PS-PEG-OCH_3	0.1	0.03 [g]	–13.3		0	0	9.1
	0.2	0.02 [g]	–12.4	–15.1	110	0.37	7.1
	0.3	0.04 [g]	–19.6	–15.5	66	0.22	9.0
	0.5	0.01 [g]	–18.0	–14.6	174	0.58	8.0
PtBMA-PEG-OCH_3	0.1	0.08	–17.1		0	0	10.3
	0.2	0.09	–13.7		0	0	9.3
	0.3	0.07	–10.5		0	0	8.6
	0.5	0.08	–19.8	–15.6	45	0.17	8.8

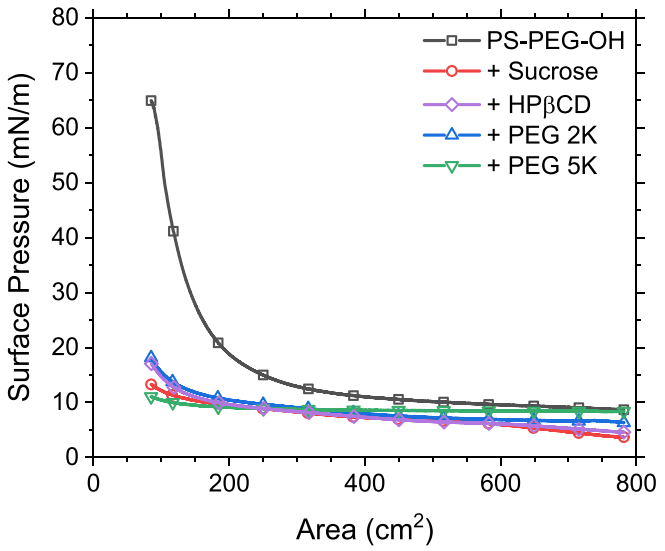

Fig. 1. Surface pressure–area isotherms of PS-PEG-OH micelles spread from formulations containing 10 % w/v excipients on pure water surfaces. These micelles were prepared using the Equilibration-Nanoprecipitation (ENP) method in a mixed solvent consisting of water and acetone, with a water volume fraction of $\varphi_{w,ENP} = 0.6$. The control measurement (black line) represents micelles without any excipients. Data points were collected at intervals of 0.3 cm^2 (solid lines), with a few data points illustrated as symbols for clarity.

PEG (2 and 4.6 kg/mol) monolayers formed by spontaneous adsorption from the subphase were 8 and 9 mN/m, respectively, (Gilányi et al., 2006) which are nearly the same as the equilibrium spreading pressure of PS-PEG-OH micelles (10 mN/m) (Kim et al., 2023). Thus, PEG-OCH_3 excipients (at a weight ratio of 20:1 to PS-PEG-OH micelles) likely occupy most of the available surface area and reduce the amount of adsorbed PS-PEG-OH micelles at the water surface. Apparently, it is difficult to use these excipients as cryo- and lyoprotectants without causing the reduction in surface activity of PLS. Moreover, the removal of these excipients from lyophilized PLS samples requires additional purification steps, such as extended dialysis, which would significantly raise manufacturing costs and associated risks.

3.2. Operation parameters for excipient-free lyophilization of PS-PEG-OH micelles

To circumvent the issues associated with excipients, our objective was to explore the optimal operating conditions for lyophilization without the need for excipients. We used the same formulation as in Section 3.1 (PS-PEG-OH micelles formulated at $\varphi_{w,ENP} = 0.6$) because it exhibited the highest PEG grafting density (σ_{PEG}) among all formulations in this study (Table 2; the effect of σ_{PEG} will be discussed later).

To assess the impact of process parameters on the quality of excipient-free lyophilization, we employed two different methods using a small-batch research-scale lyophilizer (MicroFD, Millrock Tech). Method A was designed to achieve more aggressive freezing, characterized by a faster cooling rate and a lower shelf temperature (T_{shelf}) during the freezing stage, compared to Method B (refer to Table 3 for the operation parameters of Methods A and B). Fig. 2(a) and 2(b) depict the heat flux evolution between the shelf and the vial chamber along the initial freezing trajectory, where a negative peak in the heat flux corresponds to ice crystallization. The onset of the heat flux peak, indicating ice nucleation, occurred at a lower shelf temperature (–27.2 °C) for Method A compared to Method B (–21.4 °C). The lower nucleation temperature results in a higher nucleation density and smaller crystallites. This can reduce the mechanical stress imposed by ice crystals, increase the surface area between ice and the cryo-concentrated phase, and ultimately enhance nanoparticle preservation and reconstitution (Fonte et al., 2016). Additionally, the interval between ice nucleation and the maximum rate of ice growth (indicated by shaded regions in Fig. 2(a) and 2(b)) was slightly shorter (9 min) for Method A compared to Method B (10 min), suggesting a slightly faster crystallization process when the cooling rate is doubled.

On the other hand, during the primary drying stage, both Methods A and B underwent steady-state sublimation of water until complete evaporation, as depicted in the heat flux trajectory (Figure S4). Since the T_{shelf} values used in the primary drying stage were significantly lower than the eutectic temperature ($T_{eu} = -19$ °C) in both Methods, (Kuttich et al., 2020) the quality of lyophilization (as discussed below) is unlikely to be influenced by the differences in primary drying stage parameters.

Consequently, Method A yielded better redispersibility and surface activity of the model formulations after reconstitution compared to Method B. The size increasing factor (*SIF*), defined as the ratio of the *z*-average hydrodynamic diameter ($<D_h>$) of micelles after reconstitution to that before lyophilization, was lower for Method A (Table 3), indicating less pronounced irreversible aggregation. Additionally, the difference between the Π–A isotherms of pristine and reconstituted micelles from Method A (Fig. 2(c)) was smaller than that from Method B (Fig. 2(d)), although both reconstituted micelles could achieve a high surface pressure ($\Pi_{max} \cong 70$ mN/m) at maximum surface compression. Therefore, Method A was selected as the standard lyophilization procedure for the subsequent experiments.

3.3. Effects of PEG grafting density

In polymer-grafted nanoparticles, the grafting density of hydrophilic polymers (σ_{PEG}) is a critical parameter that influences the colloidal stability of the formulations (Logie et al., 2014). A higher σ_{PEG} leads to a thicker and denser PEG brush, promoting stable dispersion (Witten and Pincus, 1986; Likos et al., 1998). This stabilizing effect of densely grafted polymer brushes is particularly relevant during the freezing stage, where ice growth reduces the available space for the particles and forces them to come into close proximity (referred to as "cryo-concentration") (Kasper and Friess, 2011). In such situations, a high σ_{PEG} is expected to protect the particles from irreversible aggregation by efficiently dampening the compressive stress. This is because the PEG brush remains partially hydrated and amorphous even below freezing temperature (see Section 3.5 for detailed discussion). It is noteworthy that Logie et al. have observed enhanced redispersibility following lyophilization, utilizing nonlinear (graft) copolymers that incorporate a higher number of PEG side chains, without the need for excipients (Logie et al., 2014).

In our system, the σ_{PEG} was systematically controlled by varying the number of block copolymer chains that constitute a micelle, also known as the aggregation number (N_{agg}). This control was achieved by applying the Equilibration-Nanoprecipitation (ENP) method with different qualities of a selective solvent (Fesenmeier et al., 2022). A higher water fraction in the ENP medium ($\varphi_{w,ENP}$) results in self-assembly with a higher N_{agg} during the process of free energy minimization, leading to larger σ_{PEG} (Nagarajan, 2015). In this study, we tested four micelle formulations with different σ_{PEG} values ranging from 7.1 to 11.3. These formulations were prepared using the same polymer but at different $\varphi_{w,ENP}$ values (Table 2). The pristine micelles exhibited uniform sizes in all formulations, and the average core diameter (D_c) increased monotonically with $\varphi_{w,ENP}$. However, the *z*-average hydrodynamic diameter ($<D_h>$) of the pristine micelles did not follow a monotonic trend with $\varphi_{w,ENP}$ due to an outlier ($\varphi_{w,ENP} = 0.2$) with the presence of significant amounts of large clusters (Table 2 and Figure S5).

The redispersibility of micelles after lyophilization and subsequent reconstitution showed a significant increase with σ_{PEG}. Transmission electron microscopy (TEM) images of the reconstituted micelles revealed that clustered micelles were larger than 100 nm at $\varphi_{w,ENP} = 0.2$ and 0.3, but decreased to approximately 50 nm at higher $\varphi_{w,ENP}$ values (Fig. 3(e–h)). Dynamic light scattering (DLS) analysis provided

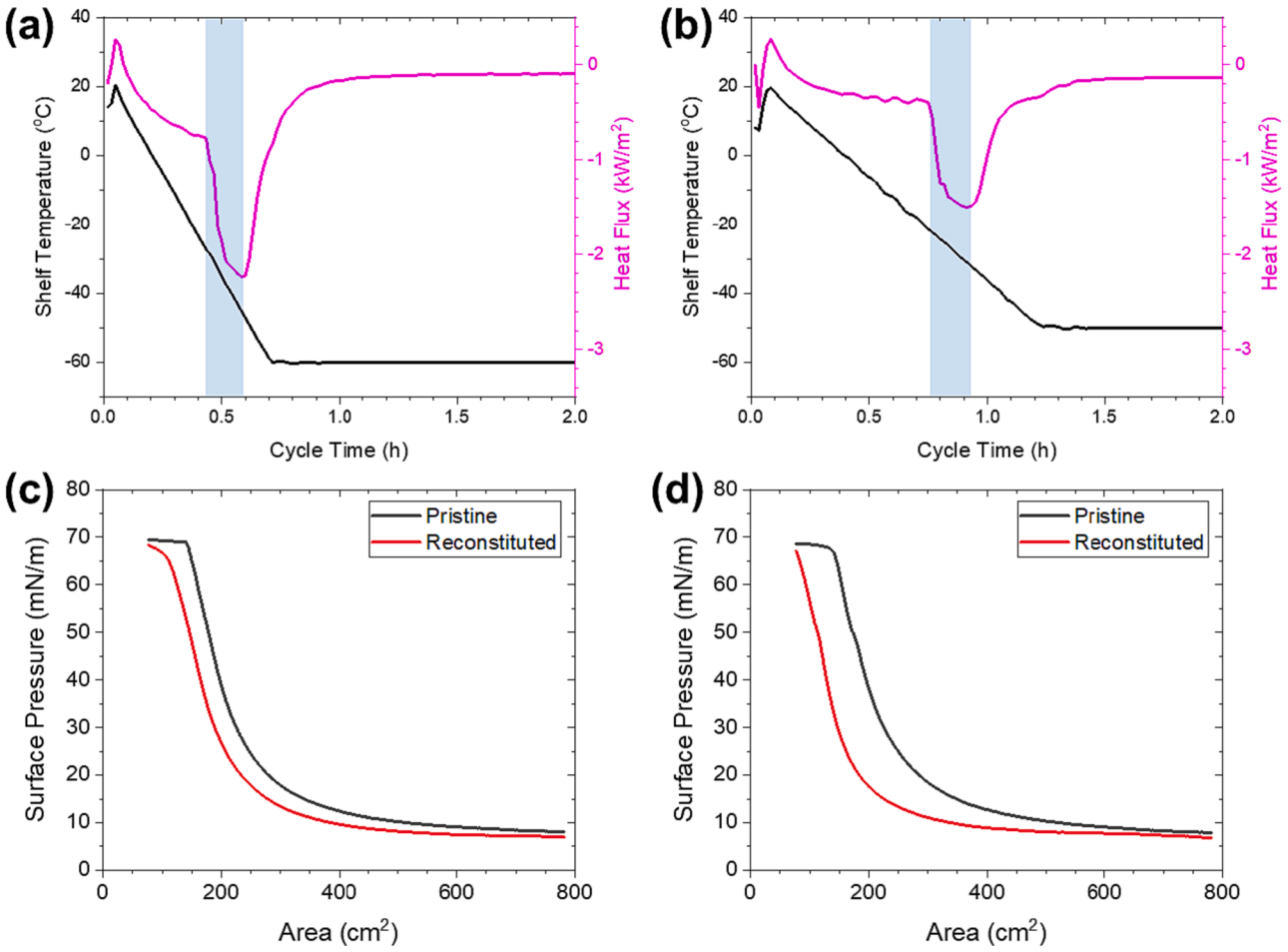

Fig. 2. **(a, b)** Shelf temperature and heat flux profiles during initial freezing stages for lyophilization Method A and Method B, respectively. The negative heat flux values indicate exothermic processes. The shaded regions represent the time intervals between the onset of nucleation and the minimum heat flux. **(c, d)** Surface pressure–area isotherms of pristine and reconstituted PS-PEG-OH micelles after lyophilization using Method A and Method B, respectively. Micelles from two separate batches, both formulated at the same $\varphi_{w,ENP} = 0.6$, were used.

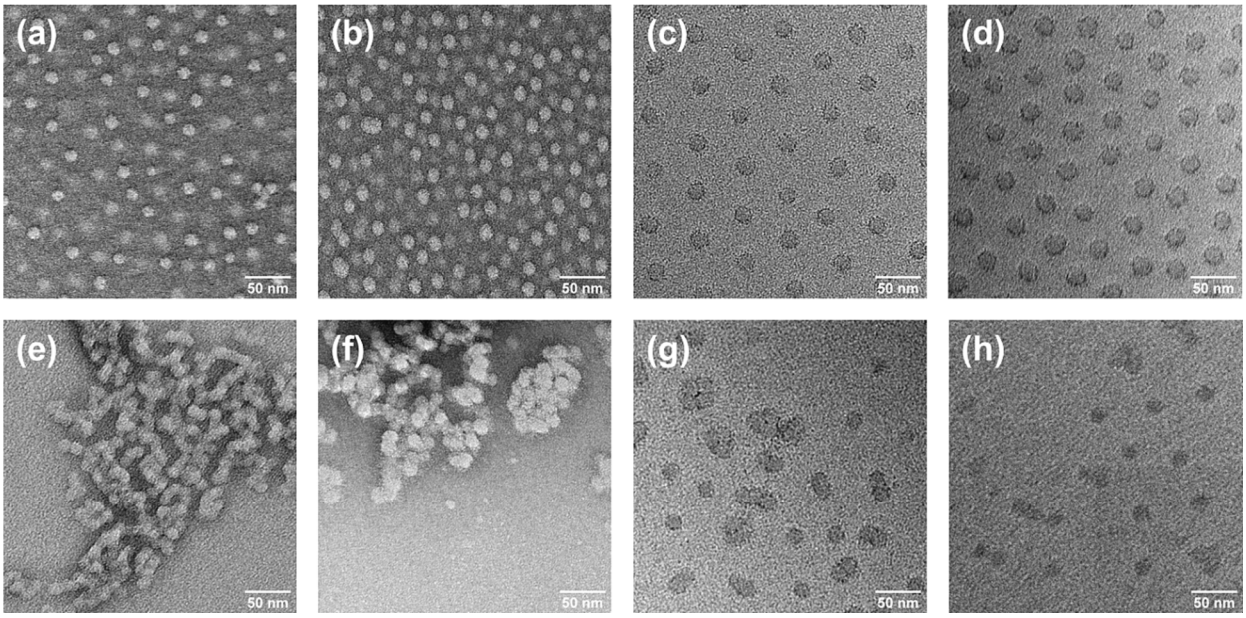

Fig. 3. TEM images of **(a–d)** pristine PS-PEG-OH micelles formulated at $\varphi_{w,ENP} = 0.2$, 0.3, 0.5, and 0.6, respectively, and **(e–h)** reconstituted micelles thereof after lyophilization and subsequent reconstitution (Method A).

consistent results, as indicated by the unanimous increase in the *z*-average hydrodynamic diameter ($<D_h>$) after lyophilization (Table 2 and Figure S5). However, the size increasing factor (*SIF*), defined as the ratio of $<D_h>$ of reconstituted micelles to pristine micelles, decreased with increasing $\varphi_{w,ENP}$ or, equivalently, increasing σ_{PEG}.

The surface activity of the reconstituted micelles exhibited a strong correlation with their redispersibility, indicating that it was preserved more effectively with higher σ_{PEG}. Fig. 4(a) and 4(b) demonstrate that the surface pressure (Π) was significantly reduced at $\varphi_{w,ENP} = 0.2$ and 0.3. This reduction can be attributed to the low availability of surface-active micelles, as clustered micelles with irregular shapes cannot expose their hydrophobic cores to the air efficiently and therefore are easily detached from the air/water surface. To quantify this effect, we introduced the concept of surface availability (*SA*), which represents the multiplication factor needed to horizontally shift the pristine isotherm to align with the reconstituted isotherm (inset in Fig. 4(a)). For example, an *SA* value of 0.36 at $\varphi_{w,ENP} = 0.2$ indicates that only 36 % of surface-active micelles are available in the reconstituted formulation relative to the pristine formulation. As the micelles become more densely grafted with PEG, the Π–*A* isotherms of the reconstituted formulations approach those of the pristine micelles (Fig. 4(c) and 4(d)), resulting in an increase in *SA* close to unity (Table 2). This clearly demonstrates the feasibility of excipient-free lyophilization when the pharmaceutical formulation consists of densely PEG-grafted micelles.

Furthermore, the lyophilized micelles in solid powder form could also be spread on the water surface and exhibited surface activity even without reconstitution. The Π–*A* isotherms of solid lyophilizates were compared with those of the reconstituted formulations in Fig. 4. It was observed that the solid lyophilizates displayed comparable or even stronger surface activity, partially due to a larger amount of material deposited on the surface (approximately 1.5 mg of solid was deposited, theoretically three times greater than the mass of polymer spread using the pristine and reconstituted aqueous formulations). Nevertheless, the feasibility of directly spreading solid lyophilizates to achieve high surface pressure (Π) is encouraging, as it may enable the delivery of PLS micelles to the alveolar space (deep inside the lungs) through inhalation, which is a more desirable approach than liquid instillation in clinical practice (Borghardt et al., 2018).

3.4. Effects of end group and core block chemistry

We expanded our study to include an analogous amphiphilic block copolymer, PS-PEG-OCH_3, which has similar block molecular weights and high surface activity. The main difference between PS-PEG-OH and

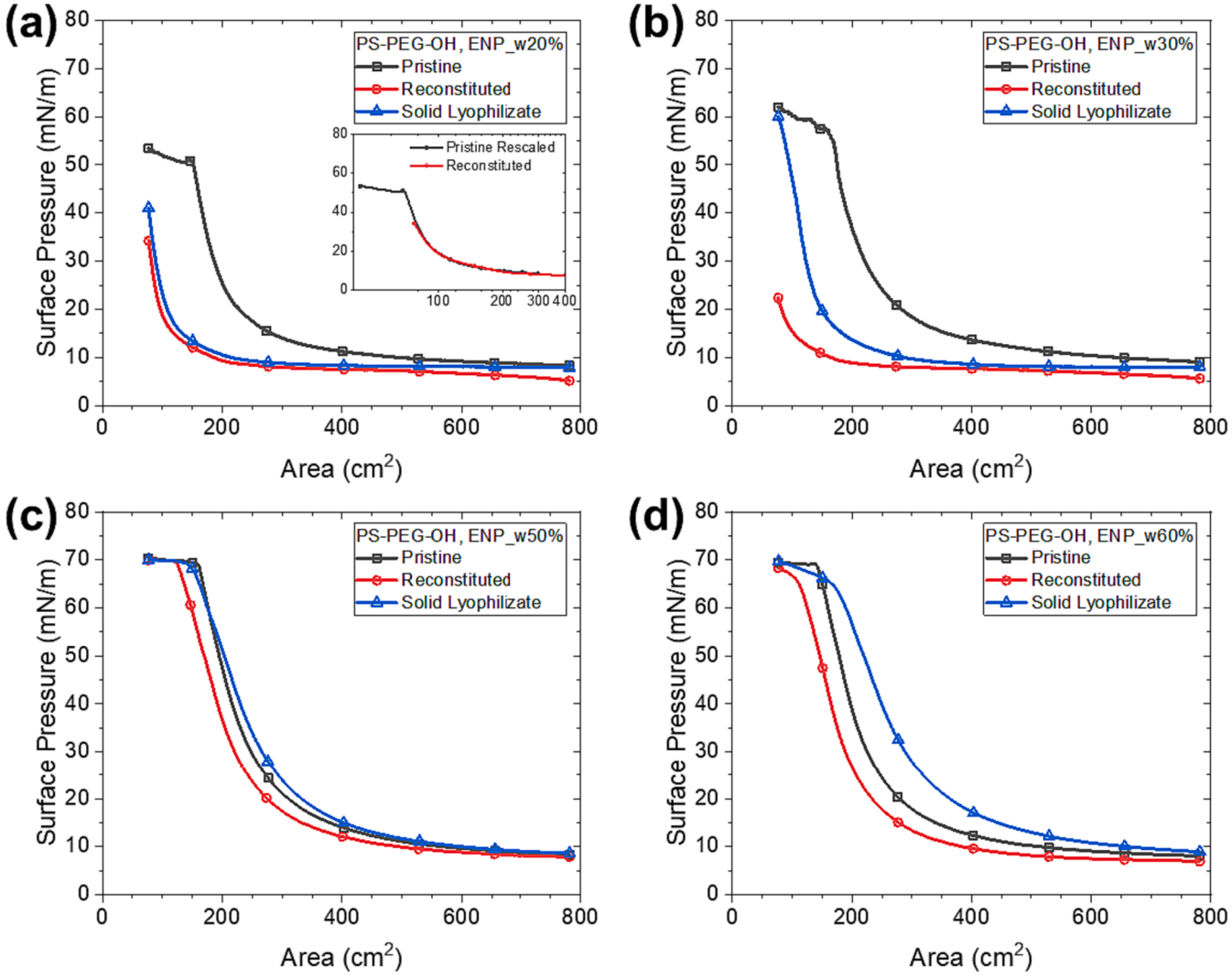

Fig. 4. Π–*A* isotherms of water-spread pristine, water-spread reconstituted, and solid-spread lyophilized PS-PEG-OH micelles at the air-water interface. Micelles were formulated at $\varphi_{w,ENP}$ = **(a)** 0.2, **(b)** 0.3, **(c)** 0.5, and **(d)** 0.6. The inset of (a) shows a representative overlap between the rescaled curve of the pristine micelles, horizontally shifted by a multipication factor ("surface availability (*SA*)") of 0.36 and the curve of the reconstituted micelles. The abscissa (area in cm^2) is presented on a logarithmic scale.

PS-PEG-OCH_3 lies in the end group chemistry of the PEG block (Table 1). Similarly to the PS-PEG-OH series, micelles were produced from PS-PEG-OH and PS-PEG-OCH_3 using the ENP method with 4 different $\varphi_{w,ENP}$ values. TEM images confirmed that all micelles were uniformly sized (Fig. 5(a–d)) and exhibited higher values of σ_{PEG} with increasing $\varphi_{w,ENP}$. However, DLS analysis revealed an unusually large $<D_h>$ for the $\varphi_{w,ENP} = 0.5$ formulation, indicating the presence of supra-micellar aggregates (Table 2 and Figure S6). Additionally, the micelles formulated at $\varphi_{w,ENP} = 0.5$ showed minimal surface activity (Fig. 6 (d)), making them unsuitable for use as PLS".

Reconstituted PS-PEG-OCH_3 micelles after lyophilization appeared as large chunks (>100 nm) in all samples (Fig. 5(e–h) and Figure S6). DLS analysis showed higher size increasing factors (*SIF*) for PS-PEG-OCH_3 micelles (*SIF* > 5), except for the $\varphi_{w,ENP} = 0.5$ formulation, which already had large aggregated clusters in the pristine state. In comparison, the SIF values for PS-PEG-OH micelles were generally smaller (*SIF* < 5) (Table 2). These systematic differences indicate that a small change in the end group chemistry of the PEG block, from hydroxy to methoxy, leads to a significantly decreased stability. This can be attributed to the bridging effect of the hydrophobic methoxy (–OCH_3) end group, which promotes closer contact between the micellar cores, especially under cryo-condensed conditions. It is interesting to note that significant aggregation of all PS-PEG-OCH_3 micelles also occurred after centrifugation (at approximately 11,000 × g for 20 min), whereas the centrifuged PS-PEG-OH micelles were easily redispersed (Table 4). Furthermore, both reconstituted and solid lyophilized forms of PS-PEG-OCH_3 micelles exhibited impaired surface activity (Fig. 6), and the surface availability (*SA*) after reconstitution was less than 0.3 in all samples, except for the $\varphi_{w,ENP} = 0.5$ formulation (Table 2).

Next, we investigated another amphiphilic block copolymer, PtBMA-PEG-OCH_3, with a different core block, for excipient-free lyophilization. In its pristine form, the PtBMA-PEG-OCH_3 micelle formulation exhibited high surface activity, generating surface pressures as high as $\Pi = 68$ mN/m in our recent study (Kim et al., 2023). TEM images confirmed that all PtBMA-PEG-OCH_3 micelles formulated at 4 different $\varphi_{w,ENP}$ appeared as uniformly sized particles (Fig. 7(a–d)). However, for the $\varphi_{w,ENP} = 0.5$ formulation, an unusually large $<D_h>$ and the inability to generate high surface pressure upon compression indicated the presence of supra-micellar aggregates (Table 2, Fig. 8, and Figure S7).

Due to the hydrophobic methoxy end group on the PEG chain of PtBMA-PEG-OCH_3, their lyophilization results were similar to those of PS-PEG-OCH_3 micelles. Reconstituted PtBMA-PEG-OCH_3 micelles after lyophilization were observed as large chunks (>100 nm) (Fig. 7(e–h)). DLS analysis consistently showed size increasing factors (*SIF*) greater than 3 for reconstituted micelles, except for the $\varphi_{w,ENP} = 0.5$ formulation where the pristine micelles already exhibited large superstructures (Table 2 and Figure S7). Once again, the pronounced aggregation in PtBMA-PEG-OCH_3 micelles after excipient-free lyophilization can be primarily attributed to the bridging effect of the methoxy (–OCH_3) end group. Consequently, the surface activity of PtBMA-PEG-OCH_3 micelles in both reconstituted and solid lyophilized forms was compromised (Fig. 8). Furthermore, the surface availability (*SA*) after reconstitution was below 0.2 in all samples, except for the $\varphi_{w,ENP} = 0.5$ formulation (Table 2). However, there were slight differences in the lyophilization results between PS-PEG-OCH_3 and PtBMA-PEG-OCH_3 micelles (excluding all $\varphi_{w,ENP} = 0.5$ formulations). The overall *SIF* values were smaller, and the solid lyophilizates exhibited higher surface activity in PtBMA-PEG-OCH_3 micelles. This suggests that PtBMA-PEG-OCH_3 micelles may be slightly more stable in maintaining colloidal dispersion. Similarly, the centrifuged PtBMA-PEG-OCH_3 micelles did not aggregate as strongly as the PS-PEG-OCH_3 micelles. However, the exact origin of this difference (in relation to the core block chemistry) is not yet fully understood.

3.5. Differential scanning calorimetry (DSC)

The redispersibility of PS-PEG-OH micelles increased as the PEG grafting density (σ_{PEG}) increased, whereas no such effect was observed in PS-PEG-OCH_3 and PtBMA-PEG-OCH_3 micelles. To further investigate the impact of the grafting density during the lyophilization cycle, we measured DSC thermograms of the aqueous micelle solutions. The solutions were cooled from 30 °C to –50 °C and subsequently heated to 30 °C at a ramping rate of ± 5 °C/min (Fig. 9(a–c)). To accurately capture the PEG/water eutectic behavior ($T_{eu} = -19$ °C), the solution concentrations were increased through centrifugal dialysis. The polymer weight fraction after centrifugation ($w_{p,analyte}$) ranged from 1 % to 10 % (Table 4). Notably, significant aggregation occurred in PS-PEG-OCH_3 micelles formulated at $\varphi_{w,ENP} = 0.1$, 0.2, and 0.5, resulting in a substantial loss of micelles in the concentrated suspensions.

DSC thermograms provided insights into the nanoscopic changes of

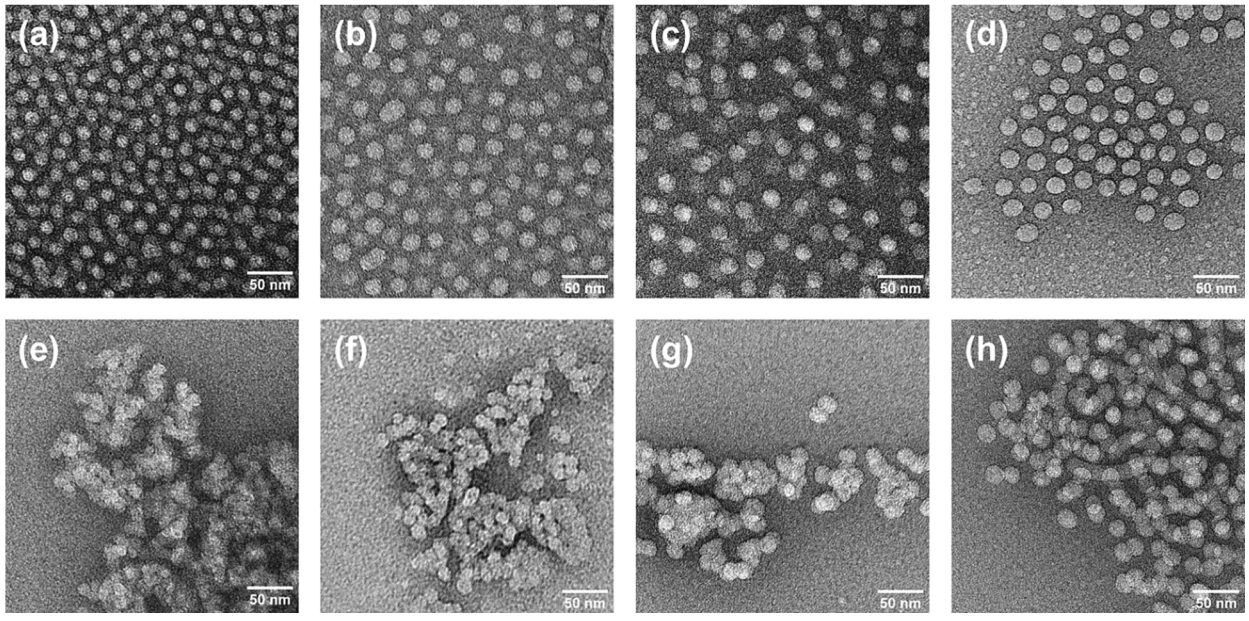

Fig. 5. TEM images of **(a–d)** pristine PS-PEG-OCH_3 micelles formulated at $\varphi_{w,ENP} = 0.1$, 0.2, 0.3, and 0.5, respectively, and **(e–h)** reconstituted micelles thereof after lyophilization and subsequent reconstitution (Method A).

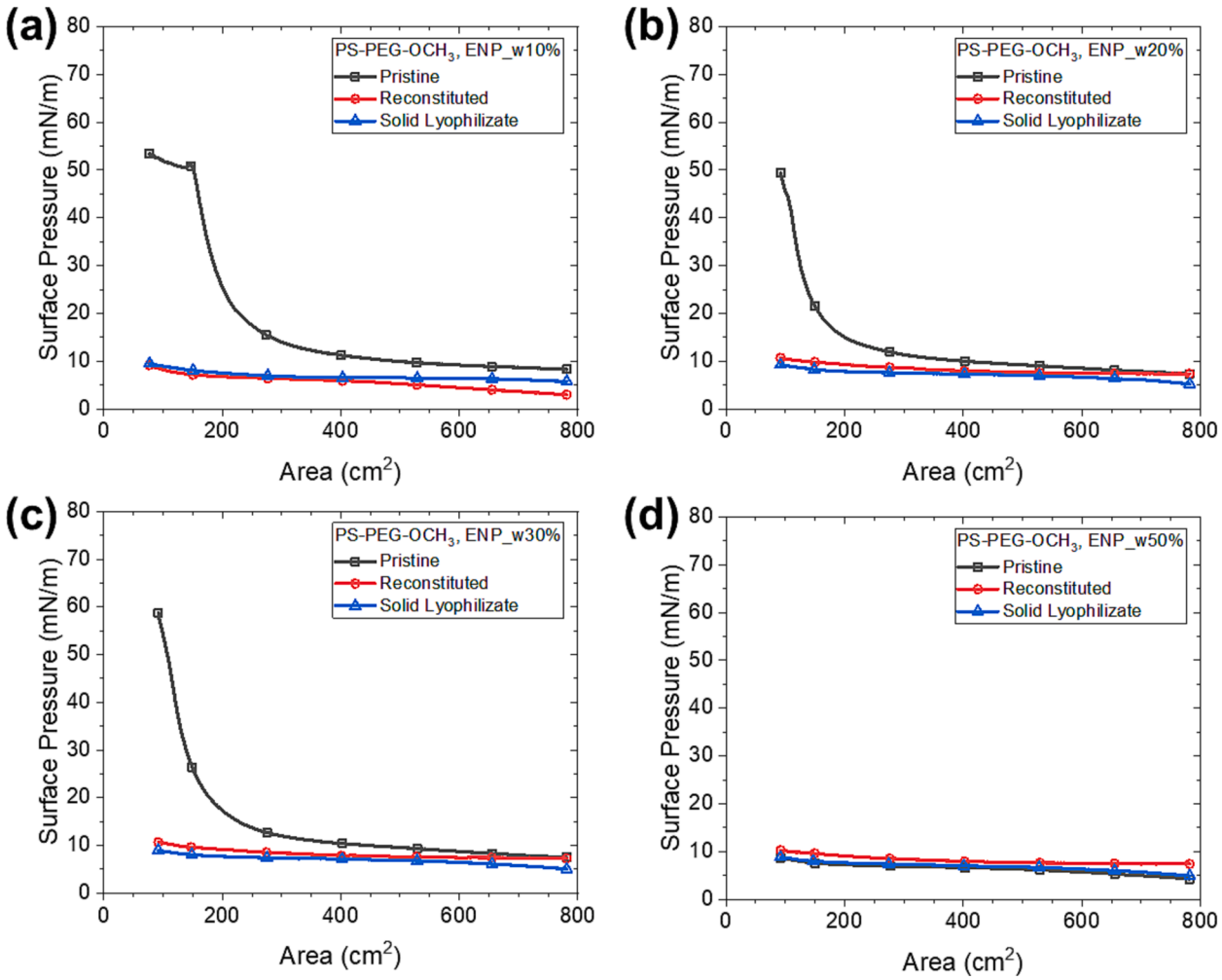

Fig. 6. *Π–A* isotherms of water-spread pristine, water-spread reconstituted, and solid-spread lyophilized PS-PEG-OCH_3 micelles at the air-water interface. Micelles were formulated at $\varphi_{w,ENP}$ = **(a)** 0.1, **(b)** 0.2, **(c)** 0.3, and **(d)** 0.5.

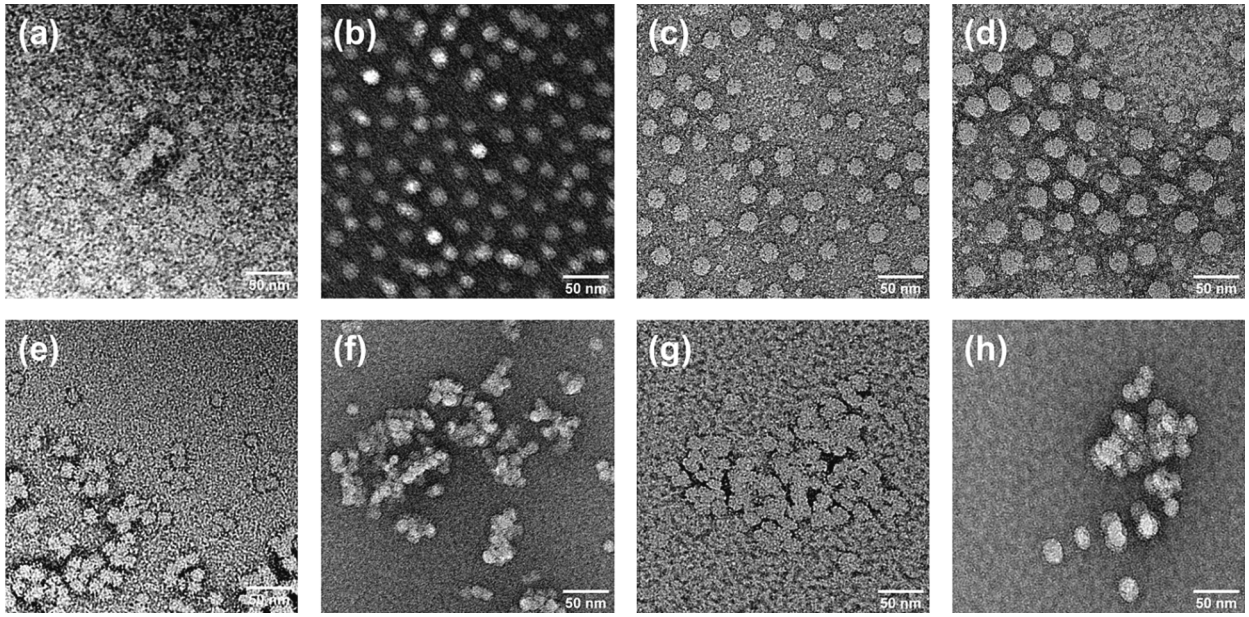

Fig. 7. TEM images of **(a–d)** pristine PtBMA-PEG-OCH_3 micelles formulated at $\varphi_{w,ENP}$ = 0.1, 0.2, 0.3, and 0.5, respectively, and **(e–h)** reconstituted micelles thereof after lyophilization and subsequent reconstitution (Method A).

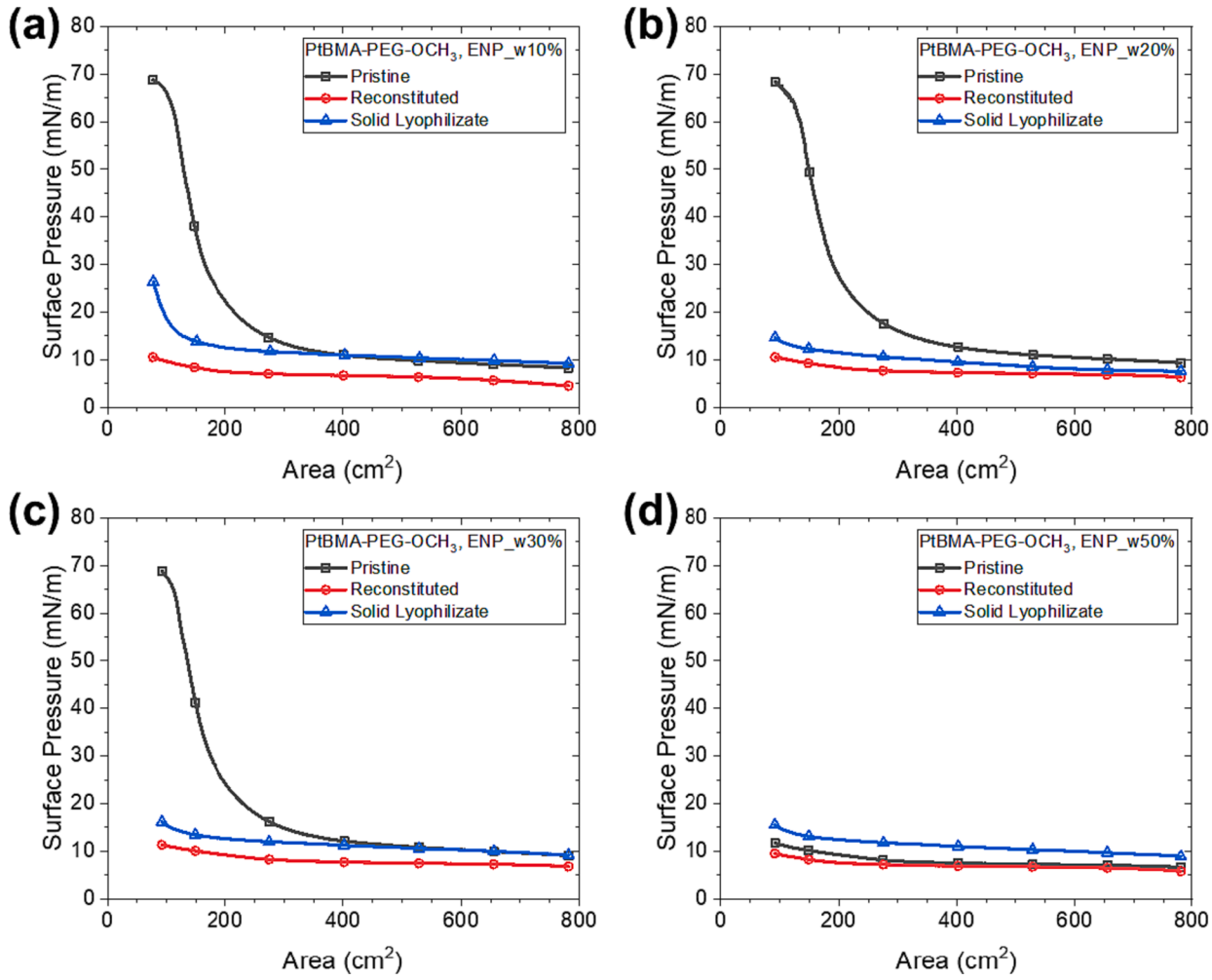

Fig. 8. *Π–A* isotherms of water-spread pristine, water-spread reconstituted, and solid-spread lyophilized PtBMA-PEG-OCH_3 micelles at the air-water interface. Micelles were formulated at $\varphi_{w,ENP}$ = **(a)** 0.1, **(b)** 0.2, **(c)** 0.3, and **(d)** 0.5.

PEG-grafted micelles in the lyophilization medium (Fig. 10(a)). Typically, phase separation between PEG and water occurs after the bulk ice crystallization at the freezing point (T_f). However, as described in previous studies, (Huang and Nishinari, 2001; Hatakeyma et al., 2007) not all PEG and water components separate into perfectly isolated crystals; instead, a substantial amount of amorphous PEG/water mixture remains even below T_{eu}. Upon heating the system from –50 °C to T_{eu}, the crystallized portion of PEG and the adjacent water melt to form a eutectic mixture. This eutectic melting is displayed in the enlarged thermograms (insets of Fig. 9(a–c)). The T_{eu} values were in close agreement (–15.5 ± 0.9 °C), but the specific heat of fusion for the eutectic mixture ($\Delta H_{eu:PEG}$) varied among the samples (Table 4). Moreover, PS-PEG-OCH_3 ($\varphi_{w,ENP}$ = 0.1) and PtBMA-PEG-OCH_3 ($\varphi_{w,ENP}$ = 0.1, 0.2, and 0.3) micelles did not exhibit eutectic melting. After surpassing T_{eu}, the bulk ice finally melted at the melting point (T_m). Most of the samples showed very similar T_m values and specific heat of melting.

We now analyze the eutectic melting in detail to evaluate the fraction of PEG segments that can freely interact with water, referred to as the hydrated PEG fraction (f_{hyd}). The distinction between hydrated and dehydrated PEG segments arises from the presence of a hydrophobic surface in block copolymer micelles. Previous studies have demonstrated that PEG brushes can form dense and nearly dehydrated layers at solid-water interfaces to reduce surface energy (Kim et al., 2018; Fesenmeier et al., 2022; Won et al., 2000). Therefore, in this study, we argue that the strongly hydrophobic PS and PtBMA cores necessitate partial dehydration of PEG brushes to form a dense layer (Fig. 10). The remaining PEG segments can be hydrated, and when a micellar suspension is frozen below T_{eu}, a portion of the hydrated PEG crystallizes, while the other portion remains amorphous as a supercooled mixture with water. The measured heat of fusion at T_{eu} ($\Delta H_{eu:PEG}$) originates from the cooperative melting of the crystalline portion of PEG in contact with ice. This heat is suppressed when the PEG brush is less hydrated, when hydrated PEG segments crystallize less during the freezing stage, or when the crystalline PEG segments lose contact with water. Therefore, $\Delta H_{eu:PEG}$ provides a convenient method to characterize the state of PEG brushes in the frozen micelle solution.

Previously, in an aqueous solution of homopolymer PEG, the empirically determined heat of melting per PEG/water eutectic mixture (ΔH_{eu}) was measured to be 142 J/(g eutectic mixture) (Huang and Nishinari, 2001). It is important to note that this value is significantly lower than the theoretical limit of ~ 217 J/g for the eutectic mixture, which was derived by considering the literature values for PEG melting enthalpy (~ 200 J/g, assuming 100% crystallinity (Lodge and Hiemenz, 2020)), water melting enthalpy (~ 334 J/g), and PEG/water mixing enthalpy (~ -53 J/g (Gunninghame and Malcolm, 1961)). Even when taking into account the semi-crystalline nature of PEG, this substantial discrepancy suggests the significant presence of amorphous water. Given the similarity in DSC methods (rapid cooling) used in both the present work (lyophilization) and the reference DSC study (-5°C/min), we can reasonably assume a comparable PEG crystallinity with the reference system. Thus, we used eq 2 with ΔH_{eu} = 142 J/(g eutectic mixture) to evaluate the f_{hyd} of the micelle samples. The results of f_{hyd}

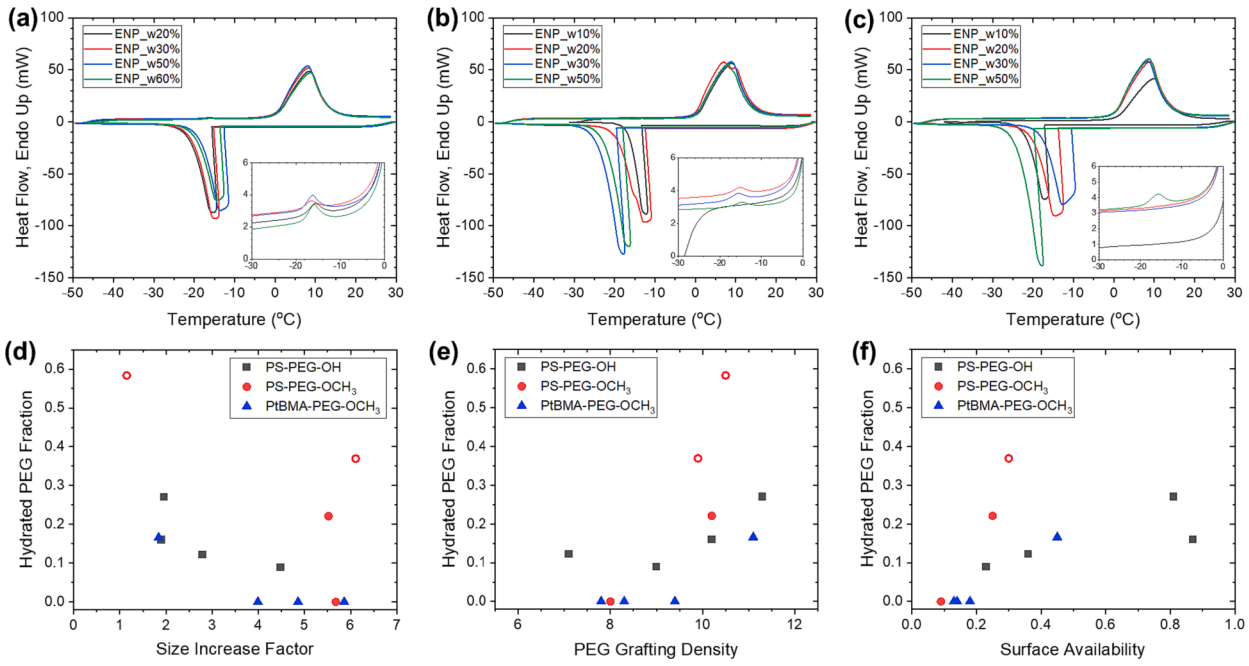

Fig. 9. **(a–c)** DSC thermograms of **(a)** PS-PEG-OH, **(b)** PS-PEG-OCH_3, and **(c)** PtBMA-PEG-OCH_3 micelle suspensions at concentrations ranging from 1 to 10 wt% (Table 4). The micelles were formulated at different $\varphi_{w,ENP}$ values as indicated in the legends. A cooling-and-heating cycle was performed at a rate of 5 °C/min. The insets provide enlarged views at the eutectic point. **(d–f)** Correlations between the fraction of hydrated PEG (evaluated from the eutectic melting enthalpy in the DSC study) and **(d)** the size increase factor (*SIF*) after lyophilization, **(e)** the non-dimensional PEG grafting density of micelles, and **(f)** the surface availability (*SA*). Open symbols represent samples with low fidelity due to low polymer concentration in the DSC analytes ($w_{p,analyte} < 0.02$).

(Table 4) show that, in most samples, the majority of PEG segments exists as a dehydrated film covering the hydrophobic core surface (i.e., $f_{hyd} < 0.5$). Nevertheless, it is rather surprising that PS-PEG-OCH_3 ($\varphi_{w,ENP} = 0.3$) and PtBMA-PEG-OCH_3 ($\varphi_{w,ENP} = 0.1$, 0.2, and 0.3) micelles lack any signature of eutectic melting. We speculate that freezing-induced massive aggregation in these samples isolated most of the PEG segments within the interior of the aggregated micellar superstructure. Such an entrapping effect may have prevented the crystallized portion of PEG from eutectic melting with water. The correlation between f_{hyd} and the size increase factor (*SIF*) obtained from the lyophilization experiment (Fig. 9(d)) supports this idea; generally, f_{hyd} is lower when the sample has a greater *SIF* (i.e., intense aggregation).

Regarding the effect of micelle structure, Fig. 9(e) illustrates a clear trend of increasing f_{hyd} with higher σ_{PEG}. In PS-PEG-OH micelles, the hydrated fraction gradually increases as σ_{PEG} increases. Since the area per PEG chain required to cover the core surface decreases with increasing σ_{PEG}, the PEG chains can allocate more segments to be hydrated after forming a dehydrated film (Fig. 10(b)). Consequently, micelles with higher σ_{PEG} exhibit thicker amorphous layers, which can effectively mitigate freezing-induced stress during the freezing stage. Similarly, in PS-PEG-OCH_3 and PtBMA-PEG-OCH_3 micelles, the eutectic melting behavior is observed only at higher σ_{PEG}, indicating that the fraction of hydrated PEG is too low at lower σ_{PEG}. However, due to the presence of hydrophobic methoxy end groups, the PEG chains now act as linkers between the cores, leading to irreversible aggregation (Fig. 10 (c)). This suggests that block copolymers with a hydrophobic end group in the PEG block are susceptible to destabilization during lyophilization. Therefore, excipient-free lyophilization is feasible only if (i) the PEG grafting density is sufficiently high to form an amorphous layer which can dissipate the external freezing stress and (ii) the PEG end group does not induce bridging interactions.

So far, we have discussed that the PEG grafting density and the endgroup at the PEG block simultaneously affect both the surface availability (*SA*) of the reconstituted micelles and the hydrated PEG fraction (f_{hyd}). Indeed, Fig. 9(f) reveals a strong correlation between f_{hyd} and *SA* even if the thermal trajectories used in the two experiments (DSC and lyophilization) were not the same. Since *SA* is the most important property in pharmaceutical surfactant formulation, this finding suggests that DSC can be used as an initial screening tool to evaluate the success of excipient-free lyophilization of PLS.

4. Conclusions

Although the use of excipients is a common practice in pharmaceutical lyophilization, there are instances where the removal of excipients becomes necessary. In our study, we focused on polymer lung surfactant (PLS) as a case in which commonly used excipients, such as saccharides and PEG, undermine the performance of the active therapeutic agent; that is, excipients impede the surface activity of PLS. We investigated the optimal conditions for excipient-free lyophilization, including material and operating parameters, using a small-batch research-scale lyophilizer. We tested micelles formulated through Equilibration-Nanoprecipitation (ENP) using three different block copolymers and four micellization equilibration water fractions ($\varphi_{w,ENP}$). The reconstitution ability after excipient-free lyophilization was assessed using various techniques, including measuring DLS hydrodynamic sizes, analyzing TEM images of the reconstituted micelles, and conducting Langmuir force balance analysis (surface pressure–area isotherms) of both the solid lyophilizates and reconstituted micelles. We found that a faster cooling rate during the freezing stage was advantageous, attributed to the formation of smaller ice crystallites, which is expected to reduce freezing stress.

Among the variations in block copolymer chemistry, we identified the PEG block end group as the most significant factor. The presence of a hydrophobic methoxy end group promoted irreversible aggregation of the micelles. For PS-PEG-OH micelles with a hydroxy end group, we observed a decrease in the size increase factor (*SIF*) and an increase in surface availability (*SA*) as the PEG grafting density increased. This can be attributed to a higher fraction of hydrated PEG in the micelle formulation, as evidenced by the specific heat of melting at the eutectic

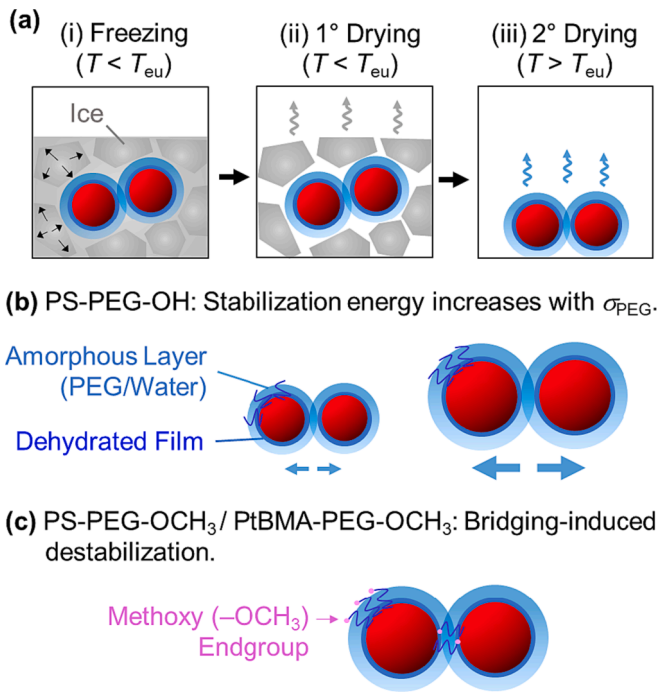

Fig. 10. (a) Schematic representation of microscopic changes in an aqueous micelle system during lyophilization stages. (i) Freezing stage: Bulk ice crystallizes, leading to the condensation and steric compression of micelles (depicted with arrows as "freezing stress"). (ii) Primary drying stage: Bulk ice sublimates, leaving behind "bound" water present as an amorphous PEG/water mixture ("amorphous layer"). (iii) Secondary drying stage: Bound water evaporates. **(b)** In aqueous media, PEG segments in the PS-PEG-OH micelle coat the hydrophobic PS surface to reduce surface energy. After forming a dehydrated PEG film, the remaining PEG segments can interact with water. The fraction of PEG segments that interact with water increases with grafting density (σ_{PEG}), enhancing the dissipating effect of the amorphous layer against freezing stress. **(c)** PS-PEG-OCH_3 and PtBMA-PEG-OCH_3 micelles exhibit similar hydrated PEG fractions compared to PS-PEG-OH micelles. However, the methoxy end groups promote particle aggregation through bridging interaction, counteracting the dissipating effect of the amorphous layer.

point (T_{eu}). In the most successful lyophilization process, which involved PS-PEG-OH formulated at $\varphi_{w,ENP} = 0.5$, the reconstituted suspension exhibited an SA of 87 %, and the solid lyophilizate perfectly reproduced the isotherm of the pristine suspension. Based on these results, we propose that the amorphous mixture of PEG/water surrounding the micellar core plays a crucial role in dissipating the freezing stress, thereby preventing irreversible aggregation of the micelles.

CRediT authorship contribution statement

Seyoung Kim: Data curation, Formal analysis, Investigation, Methodology, Validation, Visualization, Writing – original draft. **Sungwan Park:** Data curation, Formal analysis, Investigation, Validation, Visualization. **Daniel J. Fesenmeier:** Formal analysis, Investigation, Methodology. **You-Yeon Won:** Conceptualization, Formal analysis, Funding acquisition, Project administration, Supervision, Visualization, Writing – review & editing.

Declaration of Competing Interest

The authors declare that they have no known competing financial interests or personal relationships that could have appeared to influence the work reported in this paper.

Data availability

Data will be made available on request.

Acknowledgement

The authors would like to express their gratitude for the funding received from the National Science Foundation (NSF) under grant CBET-2211843. The authors also acknowledge the support provided by the Purdue University Institute for Cancer Research (PU-ICR) through an NIH NCI grant (P30 CA023168), which facilitated the use of campus-wide NMR shared resources for this research. Additionally, the authors extend their appreciation to the Purdue LyoHUB for granting access to their demonstration facility at Birck Nanotechnology Center through the LyoLaunchPad Project.

Appendix A. Supplementary material

Supplementary data to this article can be found online at https://doi.org/10.1016/j.ijpharm.2023.123476.

References

Abdelwahed, W., Degobert, G., Stainmesse, S., Fessi, H., 2006. Freeze-drying of nanoparticles: formulation, process and storage considerations. Adv. Drug Deliv. Rev. 58, 1688–1713. https://doi.org/10.1016/j.addr.2006.09.017.

Antipova, A.S., Semenova, M.G., Belyakova, L.E., 1999. Effect of sucrose on the thermodynamic properties of ovalbumin and sodium caseinate in bulk solution and at air-water interface. Colloids Surfaces B Biointerfaces. 12, 261–270. https://doi.org/10.1016/S0927-7765(98)00081-2.

Arboleya, J.C., Wilde, P.J., 2005. Competitive adsorption of proteins with methylcellulose and hydroxypropyl methylcellulose. Food Hydrocoll. 19, 485–491. https://doi.org/10.1016/J.FOODHYD.2004.10.013.

Barman, S., Davidson, M.L., Walker, L.M., Anna, S.L., Zasadzinski, J.A., 2020. Inflammation product effects on dilatational mechanics can trigger the Laplace instability and acute respiratory distress syndrome. Soft Matter 16, 6890–6901. https://doi.org/10.1039/D0SM00415D.

Borghardt, J.M., Kloft, C., Sharma, A., 2018. Inhaled therapy in respiratory disease: the complex interplay of pulmonary kinetic processes. Can. Respir. J. 2018, 1–11. https://doi.org/10.1155/2018/2732017.

Chang, L., Shepherd, D., Sun, J., Ouellette, D., Grant, K.L., Tang, X., Pikal, M.J., 2005. Mechanism of protein stabilization by sugars during freeze-drying and storage: Native structure preservation, specific interaction, and/or immobilization in a glassy matrix? J. Pharm. Sci. 94, 1427–1444. https://doi.org/10.1002/jps.20364.

Di Tommaso, C., Como, C., Gurny, R., Möller, M., 2010. Investigations on the lyophilisation of MPEG–hexPLA micelle based pharmaceutical formulations. Eur. J. Pharm. Sci. 40, 38–47. https://doi.org/10.1016/J.EJPS.2010.02.006.

Dushianthan, A., Cusack, R., Goss, V., Postle, A.D., Grocott, M.P.W., 2012. Clinical review: Exogenous surfactant therapy for acute lung injury/acute respiratory distress syndrome - where do we go from here? Crit. Care 16, 1–11. https://doi.org/10.1186/cc11512.

Fan, E., Brodie, D., Slutsky, A.S., 2018. Acute respiratory distress syndrome: advances in diagnosis and treatment. J. Am. Med. Assoc. 319, 698–710. https://doi.org/10.1001/JAMA.2017.21907.

Fesenmeier, D.J., Park, S., Kim, S., Won, Y.-Y., 2022. Surface mechanical behavior of water-spread poly(styrene)–poly(ethylene glycol) (PS–PEG) micelles at the air–water interface: Effect of micelle size and polymer end/linking group chemistry. J. Colloid Interface Sci. 617, 764–777. https://doi.org/10.1016/J.JCIS.2022.03.008.

Fesenmeier, D.J., Suresh, M.V., Kim, S., Park, S., Raghavendran, K., Won, Y.-Y., 2023. Polymer lung surfactants attenuate direct lung injury in mice. ACS Biomater Sci. Eng. 9, 2716–2730. https://doi.org/10.1021/acsbiomaterials.3c00061.

Fonte, P., Reis, S., Sarmento, B., 2016. Facts and evidences on the lyophilization of polymeric nanoparticles for drug delivery. J. Control. Release 225, 75–86. https://doi.org/10.1016/j.jconrel.2016.01.034.

Gilányi, T., Varga, I., Gilányi, M., Mészáros, R., 2006. Adsorption of poly(ethylene oxide) at the air/water interface: A dynamic and static surface tension study. J. Colloid Interface Sci. 301, 428–435. https://doi.org/10.1016/J.JCIS.2006.05.034.

Gunninghame, R.G., Malcolm, G.N., 1961. The Heats of Mixing of Aqueous Solutions of Polypropylene Glycol 400 and Polyethylene Glycol 300. J. Phys. Chem. 65 (8), 1454–1456. https://doi.org/10.1021/j100826a510.

Hatakeyma, T., Kasuga, H., Tanaka, M., Hatakeyama, H., 2007. Cold crystallization of poly(ethylene glycol)–water systems. Thermochim Acta 465, 59–66. https://doi.org/10.1016/J.TCA.2007.09.005.

Huang, L., Nishinari, K., 2001. Interaction Between Poly(ethylene glycol) and Water as Studied by Differential Scanning Calorimetry. J Polym Sci B Polym Phys. 39, 496–506. https://doi.org/10.1002/1099-0488.

Kasper, J.C., Friess, W., 2011. The freezing step in lyophilization: Physico-chemical fundamentals, freezing methods and consequences on process performance and

quality attributes of biopharmaceuticals. Eur. J. Pharm. Biopharm. 78, 248–263. https://doi.org/10.1016/j.ejpb.2011.03.010.
Kawaguchi, S., Imai, G., Suzuki, J., Miyahara, A., Kitano, T., Ito, K., 1997. Aqueous solution properties of oligo- and poly(ethylene oxide) by static light scattering and intrinsic viscosity. Polymer 38, 2885–2891. https://doi.org/10.1016/S0032-3861(96)00859-2.
Kim, S., Fesenmeier, D.J., Park, S., Torregrosa-Allen, S.E., Elzey, B.D., Won, Y.Y., 2022. Pulmonary pharmacokinetics of polymer lung surfactants following pharyngeal administration in mice. Biomacromolecules 23, 2471–2484. https://doi.org/10.1021/acs.biomac.2c00221.
Kim, S., Park, S., Fesenmeier, D., Won, Y.-Y., 2023. Surface pressure-area mechanics of water-spread poly(ethylene glycol)-based block copolymer micelle monolayers at the air-water interface: effect of hydrophobic block chemistry. Langmuir 39(38), 13546–13559. https://doi.org/10.1021/acs.langmuir.3c01574.
Kim, H.C., Won, Y.-Y., 2018. Clinical, technological, and economic issues associated with developing new lung surfactant therapeutics. Biotechnol. Adv. 36, 1185–1193. https://doi.org/10.1016/j.biotechadv.2018.03.017.
Kim, H.C., Suresh, M.V., Singh, V.V., Arick, D.Q., Machado-Aranda, D.A., Raghavendran, K., Won, Y.-Y., 2018. Polymer lung surfactants. ACS Appl. Bio Mater. 1, 581–592. https://doi.org/10.1021/acsabm.8b00061.
Kuttich, B., Matt, A., Appel, C., Stühn, B., 2020. X-ray scattering study on the crystalline and semi-crystalline structure of water/PEG mixtures in their eutectic phase diagram. Soft Matter 16, 10260–10267. https://doi.org/10.1039/D0SM01601B.
Lee, M.K., Kim, M.Y., Kim, S., Lee, J., 2009. Cryoprotectants for freeze drying of drug nano-suspensions: Effect of freezing rate. J. Pharm. Sci. 98, 4808–4817. https://doi.org/10.1002/jps.21786.
Likos, C.N., Löwen, H., Watzlawek, M., Abbas, B., Jucknischke, O., Allgaier, J., Richter, D., 1998. Star polymers viewed as ultrasoft colloidal particles. Phys. Rev. Lett. 80, 4450–4453. https://doi.org/10.1103/PhysRevLett.80.4450.
Lodge, T.P., Hiemenz, P.C., 2020. Polymer Chemistry, Third edit, CRC Press. Boca Raton. https://doi.org/10.1201/9780429190810.
Logie, J., Owen, S.C., McLaughlin, C.K., Shoichet, M.S., 2014. PEG-graft density controls polymeric nanoparticle micelle stability. Chem. Mater. 26, 2847–2855. https://doi.org/10.1021/cm500448x.
Matthay, M.A., Zemans, R.L., 2011. The acute respiratory distress syndrome: Pathogenesis and treatment. Annu. Rev. Pathol. 6, 147–163. https://doi.org/10.1146/annurev-pathol-011110-130158.
Miller, T., Van Colen, G., Sander, B., Golas, M.M., Uezguen, S., Weigandt, M., Goepferich, A., 2013. Drug loading of polymeric micelles. Pharm. Res. 30, 584–595. https://doi.org/10.1007/s11095-012-0903-5.
Nagarajan, R., 2015. “Non-equilibrium” block copolymer micelles with glassy cores: A predictive approach based on theory of equilibrium micelles. J. Colloid Interface Sci. 449, 416–427. https://doi.org/10.1016/J.JCIS.2014.12.077.
Piva, S., DiBlasi, R.M., Slee, A.E., Jobe, A.H., Roccaro, A.M., Filippini, M., Latronico, N., Bertoni, M., Marshall, J.C., Portman, M.A., 2021. Surfactant therapy for COVID-19 related ARDS: a retrospective case–control pilot study. Respir. Res. 22, 20. https://doi.org/10.1186/s12931-020-01603-w.
Saenger, W., Müller-Fahrnow, A., 1988. Cyclodextrins increase surface tension and critical micelle concentrations of detergent solutions. Angew. Chemie Int. Ed. English. 27, 393–394. https://doi.org/10.1002/ANIE.198803931.
Saez, A., Guzmán, M., Molpeceres, J., Aberturas, M.R., 2000. Freeze-drying of polycaprolactone and poly(d, l-lactic-glycolic) nanoparticles induce minor particle size changes affecting the oral pharmacokinetics of loaded drugs. Eur. J. Pharm. Biopharm. 50, 379–387. https://doi.org/10.1016/S0939-6411(00)00125-9.
Sasannejad, C., Ely, E.W., Lahiri, S., 2019. Long-term cognitive impairment after acute respiratory distress syndrome: A review of clinical impact and pathophysiological mechanisms. Crit. Care 23, 1–12. https://doi.org/10.1186/S13054-019-2626-Z.
Sim, T., Kim, J.E., Hoang, N.H., Kang, J.K., Lim, C., Kim, D.S., Lee, E.S., Youn, Y.S., Choi, H.G., Han, H.K., Weon, K.Y., Oh, K.T., 2018. Development of a docetaxel micellar formulation using poly(Ethylene glycol)–polylactide–poly(ethylene glycol) (PEG–PLA–PEG) with successful reconstitution for tumor targeted drug delivery. Drug Deliv. 25, 1371–1380. https://doi.org/10.1080/10717544.2018.1477865.
Suksiriworapong, J., Rungvimolsin, T., A-Gomol, A., Junyaprasert, V.B., Chantasart, D., 2014. Development and characterization of lyophilized diazepam-loaded polymeric micelles. AAPS PharmSciTech 15, 52–64. https://doi.org/10.1208/s12249-013-0032-4.
Torres Acosta, M.A., Singer, B.D., 2020. Pathogenesis of COVID-19-induced ARDS: Implications for an ageing population. Eur. Respir. J. 56 https://doi.org/10.1183/13993003.02049-2020.
Trenkenschuh, E., Friess, W., 2021. Freeze-drying of nanoparticles: How to overcome colloidal instability by formulation and process optimization. Eur. J. Pharm. Biopharm. 165, 345–360. https://doi.org/10.1016/j.ejpb.2021.05.024.
Willson, D.F., Notter, R.H., 2011. The Future of Exogenous Surfactant Therapy. Respir. Care 56, 1369–1388. https://doi.org/10.4187/respcare.01306.
Willson, D.F., Truwit, J.D., Conaway, M.R., Traul, C.S., Egan, E.E., 2015. The adult calfactant in acute respiratory distress syndrome trial. Chest 148, 356–364. https://doi.org/10.1378/chest.14-1139.
Witten, T.A., Pincus, A., 1986. Colloid stabilization by long grafted polymers. Macromolecules 19, 2509–2513. https://doi.org/10.1021/ma00164a009.
Won, Y.-Y., Davis, H.T., Bates, F.S., Agamalian, M., Wignall, G.D., 2000. Segment Distribution of the Micellar Brushes of Poly(ethylene oxide) via Small-Angle Neutron Scattering. J. Phys. Chem. B 104, 7134–7143. https://doi.org/10.1021/jp000457v.
Zhao, L., Wu, X., Wang, X., Duan, C., Wang, H., Punjabi, A., Zhao, Y., Zhang, Y., Xu, Z., Gao, H., Han, G., 2017. Development of excipient-free freeze-dryable unimolecular hyperstar polymers for efficient siRNA Silencing. ACS Macro Lett. 6, 700–704. https://doi.org/10.1021/acsmacrolett.7b00242.